Constraining fundamental physics with future CMB experiments

Silvia Galli,[1,2] Matteo Martinelli,[1] Alessandro Melchiorri,[1] Luca Pagano,[1] Blake D. Sherwin,[3] and David N. Spergel[4]

[1]*Dipartimento di Fisica and Sezione INFN, Università di Roma "La Sapienza," Ple Aldo Moro 2, 00185, Rome, Italy*

[2]*Laboratoire Astroparticule et Cosmologie (APC), Université Paris Diderot, 75205 Paris cedex 13, France*

[3]*Department of Physics, Princeton University, Princeton, New Jersey 08544-1001, USA*

[4]*Department of Astrophysical Sciences, Peyton Hall, Princeton University, Princeton, New Jersey 08544-1001, USA*

(Received 31 May 2010; published 1 December 2010)

The Planck experiment will soon provide a very accurate measurement of cosmic microwave background anisotropies. This will let cosmologists determine most of the cosmological parameters with unprecedented accuracy. Future experiments will improve and complement the Planck data with better angular resolution and better polarization sensitivity. This unexplored region of the CMB power spectrum contains information on many parameters of interest, including neutrino mass, the number of relativistic particles at recombination, the primordial helium abundance, and the injection of additional ionizing photons by dark matter self-annihilation. We review the imprint of each parameter on the CMB and forecast the constraints achievable by future experiments by performing a Monte Carlo analysis on synthetic realizations of simulated data. We find that next generation satellite missions such as CMBPol could provide valuable constraints with a precision close to that expected in current and near future laboratory experiments. Finally, we discuss the implications of this intersection between cosmology and fundamental physics.

DOI: 10.1103/PhysRevD.82.123504 PACS numbers: 98.80.Cq

I. INTRODUCTION

Starting with COBE's (Cosmic Background Explorer) groundbreaking detection of microwave background fluctuations [1], the past two decades have seen dramatic improvements in measurements of the microwave background temperature fluctuations (see e.g. [2–5]). Planck's highly anticipated temperature power spectrum measurements (see [6]) will further advance this program and produce significantly improved constraints on cosmological parameters.

While Planck's measurement of the anisotropy power spectrum to multipoles $\ell \sim 2000$ will extract most of the information in primordial temperature fluctuations, ongoing and planned ground-based and balloon-based experiments are exploring two important open frontiers: (a) the measurement of extremely ($\leq 5'$) small-scale temperature and polarization fluctuations [7] and (b) the search for primordial B-modes, the distinctive signature of gravitational waves from inflation, on large scales [8].

For example, balloon-borne experiments such as EBEX [9] and SPIDER [10] will improve the measurements of CMB polarization while ground-based telescopes such as the Atacama Cosmology Telescope (ACT) [11] and the South Pole Telescope [12] will extend temperature and polarization measurements to smaller, subarcminute, angular scales. Proposals for next generation CMB satellites such as CMBPol [13] or B-POL [14] are under evaluation from American and European space agencies.

What will we learn from measuring CMB temperature and polarization fluctuations on small scales? The amplitude of temperature and polarization fluctuations is determined by several different physical effects: (1) the amplitude of primordial fluctuations, (2) the evolution of the ionization fraction of the Universe at $z > 1200$, which determines the sound speed for acoustic fluctuations, (3) the evolution of the ionization fraction of the Universe at $z < 1200$, which determines the thickness of the surface of last scatter, and (4) the transition from radiation to matter domination. Moreover, while small-scale CMB fluctuations are initially pure E mode, gravitational lensing rotates E modes into B modes [15]. By measuring the pattern of small-scale E and B modes, cosmologists will be able to determine the large-scale convergence field, a direct measure of the integrated density fluctuations between redshift $z = 1100$ and $z = 0$ (see e.g. [16,17]). The convergence power spectrum is particularly sensitive to density fluctuations at $z \sim 2$, an important complement to planned optical lensing measurements that probe the evolution of density fluctuations in the $z < 1$ Universe.

The goal of this paper is to quantify the cosmological information that could come from these new data sets. This subject of investigation has already attracted several authors (see e.g. [18–20]). Here we complement these analyses in several aspects. First, while there have been many studies of the future cosmological constraints from Planck, very few papers have investigated the constraining power of combinations of future CMB data sets from different sources. Second, as we will describe in the next sections, we will consider a large set of parameters focusing on those that mainly affect the "damping tail" of the CMB angular spectrum. We consider additional parameters such as the total neutrino mass $\sum m_\nu$ (which affects the growth of structure in the late Universe), the number of additional

relativistic neutrino species $N_\nu^{\rm eff}$ (which changes the matter-radiation epoch), and possible changes in the recombination process due to changes in the fractional helium abundance Y_p, dark matter self-annihilation processes, and variations in fundamental constants such as the fine structure constant α and Newton's gravitational constant G. We will not only show the constraints on each single parameter but also the degeneracies among them.

We will consider three experimental configurations: the Planck satellite [6], the combination of Planck with ACT fitted with polarization-sensitive detectors, ACTPol, [11] and, finally, the next CMBPol satellite [13].

Recent studies have already fully demonstrated the ability of next generation satellite missions to constrain inflationary parameters [21] and the reionization history [22] in the framework of the CMBPol concept mission study (see also [23]). For this reason we will not consider primordial gravitational waves, more general reionization scenarios, or experiments that will mainly probe large angular scale polarization in this paper.

This paper will show that next generation CMB experiments can significantly improve constraints on cosmology and fundamental physics and could produce a detection of neutrino mass. The paper is structured as follows. Section II describes our analysis approach. Section III presents our analysis for improved constraints from the planned ACTPol experiment and for the proposed CMBPol experiment. Section IV discusses degeneracies between parameters and in Sec. V we present our conclusions.

II. FORECAST METHOD AND ASSUMPTIONS

We generate synthetic data sets for the Planck, ACTPol, and CMBPol experiments following the commonly used approach described, for example, in [20,24]. These data sets are generated starting from the assumption of a fiducial ''true'' cosmological model compatible with the WMAP-5 maximum likelihood parameters [4,25], i.e. with baryon density $\Omega_b h^2 = 0.0227$, cold dark matter density $\Omega_c h^2 = 0.110$, spectral index $n_s = 0.963$, and optical depth $\tau = 0.09$. This model also assumes a flat Universe with a cosmological constant, massless neutrinos with effective number $N_\nu^{\rm eff} = 3.04$, standard recombination, Helium fraction $Y_p = 0.24$, and all fundamental constants fixed to their current values (we will vary all these parameters later). Given the fiducial model, we use the publicly available Boltzmann code CAMB[1] [26] to calculate the corresponding theoretical angular power spectra C_ℓ^{TT}, C_ℓ^{TE}, C_ℓ^{EE} for temperature, cross temperature-polarization, and polarization.[2]

The synthetic data sets are then generated by considering for each C_ℓ a noise spectrum given by:

$$N_\ell = w^{-1} \exp(\ell(\ell+1) 8 \ln 2/\theta^2), \quad (1)$$

where θ is the FWHM of the beam assuming a Gaussian profile and where w^{-1} is the experimental power noise related to the detectors sensitivity σ by $w^{-1} = (\theta\sigma)^2$.

We assume that beam uncertainties are small and that uncertainties due to foreground removal are smaller than statistical errors. These are demanding assumptions; however, the experimental groups are working hard to achieve these goals.

Together with the primary anisotropy signal we also take into account information from CMB weak lensing, considering the power spectrum of the deflection field C_ℓ^{dd} and its cross correlation with temperature maps C_ℓ^{Td}. A large number of methods have been suggested for lensing extraction from CMB maps. All these methods exploit the non-Gaussian signal induced by lensing. Here we use the quadratic estimator method of Hu and Okamoto [17] that provides an algorithm for estimating the corresponding noise spectrum N_ℓ^{dd} from the observed CMB primary anisotropy and noise power spectra. This estimator is not conceived to account for the BB polarization contribution. This fact is irrelevant for the Planck satellite, as this experiment is not sensitive to the BB lensing signal, but it could be relevant for the CMBPol satellite and, possibly, for the ACTpol telescope. While algorithms that can in principle include in the forecast the lensing BB signal are already currently available, here we take the conservative approach to not include it. This leaves open the possibility to use this channel for further checks for foregrounds contamination and systematics.

We generate mock data sets with noise properties consistent, respectively, with the Planck mission (see [6]), the ACT telescope [11] and the future CMBPol experiment [13]. For the simulated Planck data set we consider the detectors at 70, 100, and 143 GHz while for ACTPol we use the single 150 GHz channel. For CMBPol we also consider the single 150 GHz channel. The experimental specifications are reported in Table I where the sensitivity σ is in units of $\Delta T/T$.

Once a mock data set is produced we compare a generic theoretical model through a likelihood $\mathcal{L}$ defined as

$$-2\ln\mathcal{L} = \sum_l (2l+1) f_{\rm sky} \left(\frac{D}{|\bar{C}|} + \ln\frac{|\bar{C}|}{|\hat{C}|} - 3 \right), \quad (2)$$

where D is defined as in [24]:

$$\begin{aligned} D = {} & \hat{C}_\ell^{TT} \bar{C}_\ell^{EE} \bar{C}_V^{dd} + \bar{C}_\ell^{TT} \hat{C}_\ell^{EE} \bar{C}_\ell^{dd} + \bar{C}_\ell^{TT} \bar{C}_\ell^{EE} \hat{C}_\ell^{dd} \\ & - \bar{C}_\ell^{TE} (\bar{C}_\ell^{TE} \hat{C}_\ell^{dd} + 2 \hat{C}_\ell^{TE} \bar{C}_\ell^{dd}) \\ & - \bar{C}_\ell^{Td} (\bar{C}_\ell^{Td} \hat{C}_\ell^{EE} + 2 \hat{C}_\ell^{Td} \bar{C}_\ell^{EE}), \end{aligned} \quad (3)$$

where $\bar{C}_l$ and $\hat{C}_l$ are the fiducial and theoretical spectra plus noise, respectively, and $|\bar{C}|$, $|\hat{C}|$ denote the determinants of

[1] http://camb.info/.

[2] Note that we do not consider the B mode lensing channel; we will discuss this choice later in this section.

TABLE I. Planck [6], ACTPol [11], and CMBPol [13] experimental specifications. Channel frequency is given in GHz, FWHM in arc minutes and noise per pixel for the Stokes I (ΔT/T), Q, and U parameters (ΔP/T) is in $[10^6 \mu\mathrm{K/K}]$, where $\mathrm{T} = \mathrm{T_{CMB}} = 2.725\mathrm{K}$. In the analysis, we assume that beam uncertainties and foreground uncertainties are smaller than the statistical errors in each of the experiments.

Experiment	Channel	FWHM	$\Delta T/T$	$\Delta P/T$
Planck	70	14'	4.7	6.7
$f_{\mathrm{sky}} = 0.85$	100	10'	2.5	4.0
	143	7.1'	2.2	4.2
ACTPol	150	1.37'	5.4	7.6
$f_{\mathrm{sky}} = 0.097$				
CMBPol	150	5.6'	0.037	0.052
$f_{\mathrm{sky}} = 0.72$				

the theoretical and observed data covariance matrices respectively,

$$|\bar{C}| = \bar{C}_\ell^{TT}\bar{C}_\ell^{EE}\bar{C}_\ell^{dd} - (\bar{C}_\ell^{TE})^2\bar{C}_\ell^{dd} - (\bar{C}_\ell^{Td})^2\bar{C}_\ell^{EE}, \quad (4)$$

$$|\hat{C}| = \hat{C}_\ell^{TT}\hat{C}_\ell^{EE}\hat{C}_\ell^{dd} - (\hat{C}_\ell^{TE})^2\hat{C}_\ell^{dd} - (\hat{C}_\ell^{Td})^2\hat{C}_\ell^{EE}, \quad (5)$$

and finally f_{sky} is the sky fraction sampled by the experiment after foregrounds removal.

We derive constraints from simulated data using a modified version of the publicly available Markov Chain Monte Carlo package COSMOMC [27] with a convergence diagnostic based on the Gelman and Rubin statistic performed on eight chains. We sample the following *six*-dimensional set of cosmological parameters, adopting flat priors on them: the physical baryon and cold dark matter density fractions, $\omega_b = \Omega_b h^2$ and $\omega_c = \Omega_c h^2$, the ratio of the sound horizon to the angular diameter distance at decoupling θ_S, the scalar spectral index n_S, the overall normalization of the spectrum A_s at $k = 0.002\ \mathrm{Mpc}^{-1}$, and the optical depth to reionization τ. We then perform the analysis sampling in addition to one of the following parameters at a time: the total mass of neutrinos $\sum m_\nu$, the primordial helium abundance Y_p, and the dark energy equation of state w. We also consider parameters that can change the process of recombination: the dark matter self-annihilation rate p_{ann}, a variation in the fine structure constant α/α_0 and in Newton's constant $\lambda_G = G/G_0$, where α_0 and G_0 are the currently measured values. For these latter parameters we choose to sample the Hubble constant H_0 instead of θ_S since these parameters are derived assuming standard recombination. We also discuss some of the degeneracies that might arise if more than one additional parameter is considered to vary at the same time. We briefly explain how the constraints might be affected and present, in the most relevant cases, the constraints obtained by varying the six ΛCDM standard parameters and two additional parameters.

We use a cosmic age top-hat prior with $10\ \mathrm{Gyr} \leq t_0 \leq 20\ \mathrm{Gyr}$. Furthermore, we consider adiabatic initial conditions and we impose flatness.

In what follows we will consider temperature and polarization power spectrum data up to $\ell_{\mathrm{max}} = 2500$, due to possible unresolved foreground contamination at smaller angular scales and larger multipoles. Measurements of small-scale temperature fluctuations by ACT [28] and SPT [29] confirm that extragalactic foregrounds will limit precision measurements of primordial temperature fluctuations to $\ell < 2500$. Even if these foregrounds could be removed, kinetic Sunyaev-Zel'dovich fluctuations would provide a limiting source of confusion that will be difficult to model and impossible to remove as it has the same spectral shape as primordial fluctuations. Small-scale polarization measurements offer our best hope to probe the early Universe on angular scales of $\ell = 2000$–4000: dusty galaxies are thought to be only 1%–2% polarized [30]. We expect that secondary fluctuations should produce minimal polarization fluctuations and therefore that polarization will provide a way of probing the primordial spectrum at small scales. We have checked that for the parameters considered here, the constraints were not sensitive to whether the cutoff was set at $\ell_{\mathrm{max}} = 2500$ or 3500.

III. RESULTS

A. Constraints on the "standard" six parameters Λ-CDM scenario

In Table II we report the future constraints on the parameters of a ''minimal'' cosmological model. Together with the standard deviations on each parameter we also report, for ACTPol and CMBPol, the improvement factor for each parameter defined as the ratio $\sigma_{\mathrm{Planck}}/\sigma$ where σ is the error from Planck + ACTPol or CMBPol and σ_{Planck} is the constraint from Planck.

As we can see in the table, the combination of Planck with ACTPol will improve by a factor $\sim$1.3 the constraints on most of the parameters derived from Planck alone. CMBPol will improve by a factor $\sim$4 the constraints on the baryon density, H_0 and θ_s, while the constraints on parameters as n_s and τ are improved by a factor $\sim$2.

B. Future constraints on neutrino masses

The detection of the absolute mass scale of the neutrino is one of the major goals of experimental particle physics. However, cosmology could provide an earlier, albeit model-dependent, detection. CMB power spectra are sensitive to a total variation in neutrino mass eigenstates Σm_ν (see e.g. [31–33]) but cannot discriminate between the mass of a single neutrino flavor (see e.g. [34]) because of degeneracies with other parameters. Inclusion of massive neutrinos increases the anisotropy at small scales because the decreased perturbation growth contributes to the photon energy density fluctuation. Moreover, gravitational

TABLE II. 68% C.L. errors on cosmological parameters from future surveys. A standard, six parameters Λ-CDM scenario is assumed. The numbers in brackets show the improvement factor $i = \sigma_{\rm Planck}/\sigma$ with respect to the Planck experiment.

Parameter uncertainty	Planck	Planck + ACTPol		CMBPol	
$\sigma(\Omega_b h^2)$	0.00013	0.000093	(1.4)	0.000034	(3.8)
$\sigma(\Omega_c h^2)$	0.0010	0.00077	(1.3)	0.00027	(3.7)
$\sigma(\theta_s)$	0.00026	0.00018	(1.4)	0.000052	(5.0)
$\sigma(\tau)$	0.0042	0.0035	(1.2)	0.0022	(1.9)
$\sigma(n_s)$	0.0031	0.0023	(1.3)	0.0014	(2.2)
$\sigma(\log[10^{10}As])$	0.013	0.0098	(1.3)	0.0055	(2.4)
$\sigma(H_0)$	0.53	0.37	(1.4)	0.12	(4.4)

TABLE III. 68% C.L. errors on cosmological parameters in the case of massive neutrinos. The numbers in brackets show the improvement factor $\sigma_{\rm Planck}/\sigma$ with respect to the Planck experiment. The entries for $\sigma(\sum m_\nu)$ are upper limits (<) at 68% C.L.

Parameter uncertainty	Planck	Planck + ACTPol		CMBPol	
$\sigma(\Omega_b h^2)$	0.00014	0.000095	(1.5)	0.000033	(4.2)
$\sigma(\Omega_c h^2)$	0.0017	0.0012	(1.4)	0.00071	(2.4)
$\sigma(\theta_S)$	0.00028	0.00020	(1.4)	0.000062	(4.5)
$\sigma(\tau)$	0.0042	0.0038	(1.1)	0.0023	(1.8)
$\sigma(n_S)$	0.0034	0.0025	(1.4)	0.0016	(2.1)
$\sigma(\log[10^{10}A_S])$	0.013	0.011	(1.2)	0.0065	(2.0)
$\sigma(\sum m_\nu)$	<0.16	<0.10	(1.6)	<0.05	(3.2)

lensing leads to smoothing of the acoustic peaks and enhancement of power on the damping tail of the power spectrum; the amount of lensing is also connected to the neutrino mass (see e.g. [35]).

Current oscillation experiments provide essentially two mass differences for the neutrino mass eigenstates: $\Delta m^2_{\rm solar} \sim 8 \times 10^{-5}$ eV^2 and $\Delta m^2_{\rm atm} \sim 2.5 \times 10^{-3}$ eV^2 (see e.g. [36] and references therein). An inverted hierarchy in the neutrino mass eigenstates predicts a lower limit to the total neutrino mass of about $\sum m_\nu \geq 0.10$ eV while a direct hierarchy predicts $\sum m_\nu \geq 0.05$ eV. The goal for CMB experiments is therefore to have a sensitivity better than $\sum m_\nu \leq 0.10$ eV for possibly ruling out the inverted hierarchy and better than $\sum m_\nu \leq 0.05$ eV for a definitive detection of neutrino mass.

As we can see from Table III the expected sensitivity from Planck and Planck + ACTPol is sufficient to find the neutrino mass in the inverted hierarchy case, while CMBPol could possibly also measure it in the direct hierarchy case. In particular, the combination of ACTPol data with Planck is expected to improve the bound on the neutrino mass by a factor of 1.6 while CMBPol can improve it by a factor of more than 3. These limits are far better than those expected from future laboratory experiments. The expected upper limit expected from the KATRIN [37] beta decay experiment is $m_{\nu_e} < 0.2$ eV at 90% C.L., which roughly translates to an upper limit of $\sum m_\nu < 0.48$ eV at 1 standard deviation (see [38]). Planck and Planck + ACTPol will explore the same energy scale, providing a great opportunity for confirming or anticipating a mass detection from KATRIN. Planck alone will also falsify or confirm the claim of detection of the absolute scale of the neutrino mass from the Heidelberg-Moscow neutrinoless double beta decay experiment with an effective electron neutrino mass in the range 0.2 eV $< m_{\nu_e} <$ 0.6 eV at 99.73% C.L. [39].

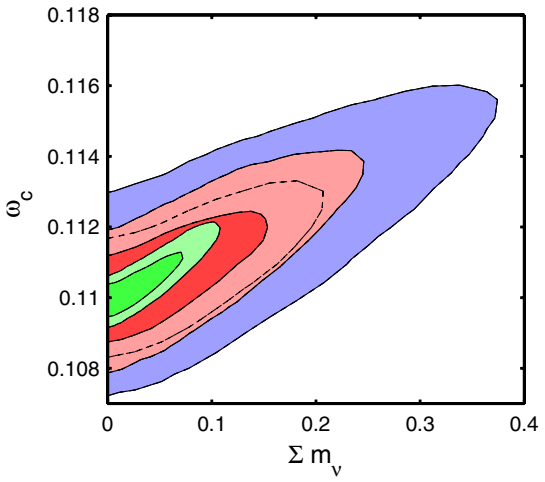

FIG. 1 (color online). 68% and 95% likelihood contour plots on the $\sum m_\nu$–ω_c plane for Planck (blue), Planck + ACTPol (red), and CMBPol (green).

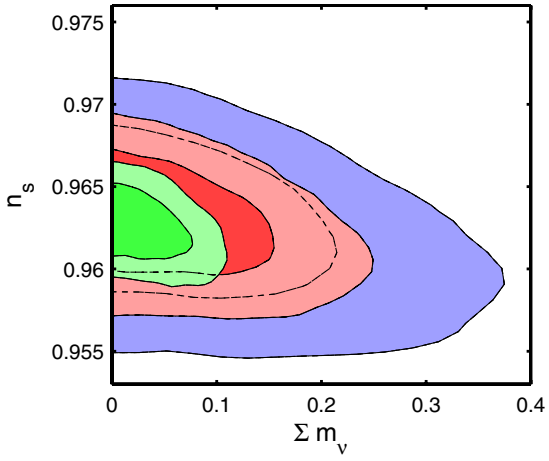

FIG. 2 (color online). 68% and 95% likelihood contour plots on the $\sum m_\nu$–n_s plane for Planck (blue), Planck + ACTPol (red), and CMBPol (green).

Future double beta decay experiments such as MARE [40] should sample mass scales of the order of $m_{\nu_e} \sim 0.2$ eV. These experiments, if combined with Planck and Planck + ACTPol constraints, could provide extremely valuable information on neutrino physics. For example, a CMB detection of a neutrino mass not confirmed by double beta decay experiments would rule out neutrinos as majorana-like particles.

Including a neutrino mass in the determination of the cold dark matter density ω_c results in an uncertainty that is nearly doubled with respect to the standard analysis, as we can see by comparing Table III with Table II. Moreover, the constraints on n_s are also affected. We show in Figs. 1 and 2 the two-dimensional likelihood contour plots at 68% and 95% confidence level in the Σm_ν vs ω_c and vs n_s planes, respectively. As we can see, a non-negligible neutrino mass has positive correlation with higher values of the cold dark matter abundance and lower values of the scalar spectral index.

C. Future constraints on extra background of relativistic particles

An additional background of relativistic (and noninteracting) particles can be parametrized by introducing an effective number of neutrino species $N_\nu^{\rm eff}$. This additional background changes the CMB anisotropies through time variations of the gravitational potential at recombination due to the presence of this non-negligible relativistic component (the so-called early integrated Sachs Wolfe effect). The main consequence is an increase in the small-scale CMB anisotropy (see e.g. [41]). The results are reported in Table IV.

As we can see, combining ACTPol with Planck will improve the constraint on $N_{\rm eff}$ by a factor of 1.4 while CMBPol could improve it by a factor of ~3.7. Comparing with the results in Table II, the inclusion of a background of relativistic particles strongly weakens the constraints on n_s, ω_b, ω_c, and θ_s. As we can see from Figs. 3–6 there is indeed a strong positive correlation between $N_\nu^{\rm eff}$ and these parameters (negative for θ_s).

While adding ACT data will improve the constraints by a factor ~1.4, CMBPol can provide constraints that could give valuable information on the physics of neutrino decoupling from the photon-baryon primordial plasma. As it is well known, the standard value of neutrino parameters $N_{\rm eff} = 3$ should be increased to $N_{\rm eff} = 3.04$ due to an additional contribution from a partial heating of neutrinos during the electron-positron annihilations (see e.g. [42]). This effect, expected from standard physics, could be tested by the CMBPol experiment, albeit at just 1 standard deviation. However, the presence of nonstandard neutrino-electron interactions may enhance the entropy transfer from electron-positron pairs into neutrinos instead of photons, up to a value of $N_{\rm eff} = 3.12$ ([43]). This value could be discriminated by CMBPol from $N_{\rm eff} = 3$ at ~3 standard deviations, shedding new light on nonstandard neutrino-electron interactions models.

TABLE IV. 68% C.L. errors on cosmological parameters in the case of extra background of relativistic particles $N_{\rm eff}$. The numbers in brackets show the improvement factor $\sigma_{\rm Planck}/\sigma$ with respect to the Planck experiment.

Parameter uncertainty	Planck	Planck + ACTPol		CMBPol	
$\sigma(\Omega_b h^2)$	0.00020	0.00016	(1.3)	0.000048	(4.1)
$\sigma(\Omega_c h^2)$	0.0025	0.0017	(1.5)	0.00058	(4.3)
$\sigma(\theta_s)$	0.00044	0.00030	(1.3)	0.000075	(5.9)
$\sigma(\tau)$	0.0043	0.0038	(1.1)	0.0023	(1.9)
$\sigma(n_s)$	0.0073	0.0056	(1.3)	0.0026	(2.8)
$\sigma(\log[10^{10} A_s])$	0.019	0.014	(1.4)	0.0078	(2.4)
$\sigma(N_{\rm eff})$	0.18	0.13	(1.4)	0.044	(4.1)

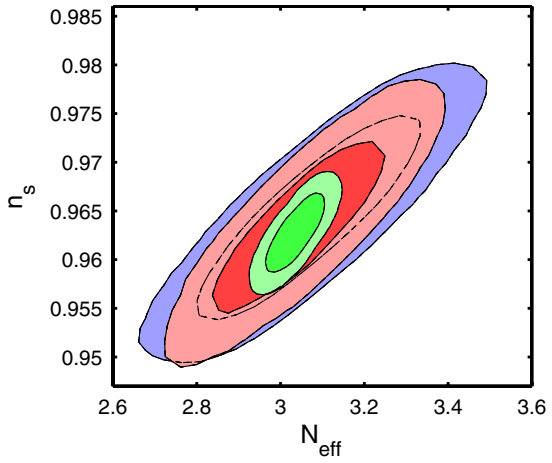

FIG. 3 (color online). 68% and 95% likelihood contour plots on the $N_{\rm eff}$–n_s plane for Planck (blue), Planck + ACTPol (red), and CMBPol (green).

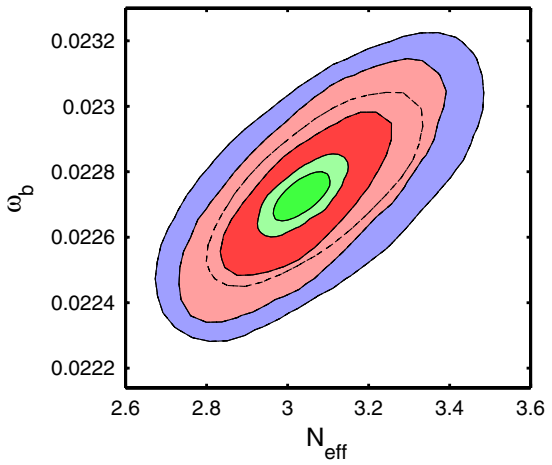

FIG. 4 (color online). 68% and 95% likelihood contour plots on the $N_{\rm eff}$–ω_b plane for Planck (blue), Planck + ACTPol (red), and CMBPol (green).

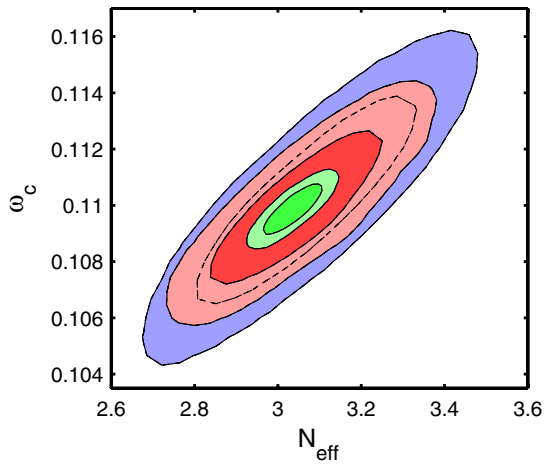

FIG. 5 (color online). 68% and 95% likelihood contour plots on the $N_{\rm eff}$–ω_c plane for Planck (blue), Planck + ACTPol (red), and CMBPol (green).

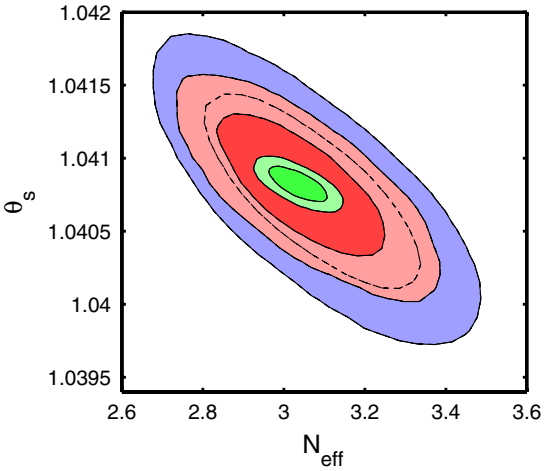

FIG. 6 (color online). 68% and 95% likelihood contour plots on the $N_{\rm eff}$–θ_s plane for Planck (blue), Planck + ACTPol (red), and CMBPol (green).

D. Future constraints on dark matter self-annihilation

Annihilating particles affect the ionization history of the Universe in three different ways: the interaction of the shower produced by the annihilation with the thermal gas can ionize the gas, induce Ly–α excitation of the hydrogen, and heat the plasma. The first two modify the evolution of the free electron fraction x_e, the third affects the temperature of baryons ([44–47]).

The rate of energy release $\frac{dE}{dt}$ per unit volume by a relic self-annihilating dark matter particle is given by

$$\frac{dE}{dt}(z) = \rho_c^2 c^2 \Omega_{\rm DM}^2 (1+z)^6 p_{\rm ann}, \tag{6}$$

$$p_{\rm ann} = f \frac{\langle \sigma v \rangle}{m_\chi}, \tag{7}$$

where $n_{\rm DM}(z)$ is the relic dark matter (DM) abundance at a given redshift z, $\langle \sigma v \rangle$ is the effective self-annihilation rate and m_χ the mass of our dark matter particle, $\Omega_{\rm DM}$ is the dark matter density parameter, and ρ_c is the critical density of the Universe today; the parameter f indicates the fraction of energy which is absorbed *overall* by the gas, under the approximation that the energy absorption takes place locally. The CMB is sensitive to the combined parameter $p_{\rm ann}$ only. The greater $p_{\rm ann}$, the higher the fraction of free electrons surviving after recombination, which widens the peak of the visibility function and dampens the peaks of the temperature and polarization angular power spectra.

In order to include the effects of this energy injection in the standard recombination model, we have modified the RECFAST routine [48] in the CAMB code [26], following the prescription described in [44].

As we can see by comparing the entries in Table V with the results in Table II, the inclusion of dark matter self-annihilation does not substantially affect the constraints on the other parameters.

As shown in Galli *et al.* [44], WMAP5 data already puts interesting constraints on dark matter annihilation, namely $p_{\rm ann} = 2.4 \times 10^{-6}$ $[m^3/{\rm s/Kg}]$ at 95% C.L. This result disfavors dark matter annihilation as the main cause of the anomalies in the cosmic ray positron to electron fraction measured by PAMELA [49] and in the energy spectrum of cosmic ray electrons measured by ATIC [50] and less evidently by FERMI [51]. Slatyer *et al.* [52] examined the constraining power of this result on weakly interacting massive particle-like dark matter models that fit the excesses in the data. In these models, particles annihilate in leptons and pions both directly and through a new GeV-scale state. They showed that most of these models are excluded by WMAP5 at almost $2-\sigma$ C.L.

Results reported in Table V will exclude these models at more than $\sim 10-\sigma$ C.L. for Planck and Planck + ACT and at $\sim 20-\sigma$ for CMBPol, as shown in Fig. 7.

It is also interesting to notice that the constraints obtained by CMBpol are comparable to those obtained by a cosmic variance limited experiment with angular resolution comparable to Planck and without lensing extraction. In fact, such a cosmic variance limited experiment gives a constraint of $p_{\rm ann} = 5 \times 10^{-8}$ [44], comparable to the one reported in Table V for CMBpol. Finally, it is worth noting that adding small-scale data from ACT improves the constraints obtained with Planck only data by just $\sim 10\%$.

E. Future constraints on helium abundance

As recently shown by several authors ([5,53–55]) the small-scale CMB anisotropy spectrum can provide a powerful method for accurately determining the primordial ^{4}He abundance. Current astrophysical measurements of primordial fractional abundance $Y_p = {}^4{\rm He}/(H + {}^4{\rm He})$ can be contained in the conservative estimate of $Y_p = 0.250 \pm 0.003$ (see e.g. [56]).

As we can see from Table VI, the Planck satellite mission alone will not reach this accuracy, even when combined with ACT. However, it is important to note that the helium abundance in the big bang nucleosynthesis scenario is a growing function of $N_{\rm eff}$ and the baryon density.

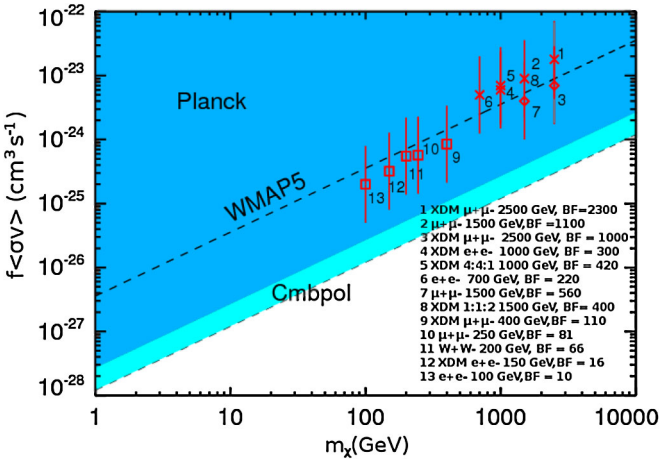

FIG. 7 (color online). Constraints on the self-annihilation cross section at recombination $(<\sigma v>)_{zr}$ times the gas-shower coupling parameter f. The dark grey (dark blue) area is excluded by Planck at 95% C.L., whereas the lightest grey (lightest blue) area indicates the additional parameter space excluded by CMBpol. Planck + ACT constraint is not shown as it is only 20% tighter than the Planck constraint. The dashed line represents the current constraints given by the WMAP5 data [44]. The data points are taken from [52] (based on the results of [80,81]), and indicate the positions of models of dark matter particles that fit the observed cosmic ray excesses for PAMELA data (squares), Planck + FERMI (diamods), and Planck + ATIC (crosses). The ratios appearing in the legend indicate models of particles that annihilate through an intermediate light state to electrons, muons, and pions in the given ratio. Error bars indicate astrophysical uncertainties in the cross section boost factor. We refer to [52] for further details on these models.

A change in $\Delta N_{\rm eff} \sim 1$ could produce a $\sim 5\%$ variation in Y_p that could be measurable by Planck or Planck + ACTPol. Moreover, a CMBPol-like experiment has the potential of reaching a precision comparable with current astrophysical measurements. This will open a new window of research for testing systematics in current primordial helium determinations.

Comparing the results in Table VI with the constraints obtained in the case of a standard analysis in Table II, it is

TABLE V. 68% C.L. errors on cosmological parameters in the case of dark matter annihilation. The entries for $\sigma(p_{\rm ann})$ are upper limits ($<$) at 95% C.L. The parameter $p_{\rm ann}$ is measured in $[m^3/{\rm s/Kg}]$. The numbers in brackets show the improvement factor $\sigma_{\rm Planck}/\sigma$ with respect to the Planck experiment.

Parameter uncertainty	Planck	Planck + ACTPol		CMBPol	
$\sigma(\Omega_b h^2)$	0.00013	0.000094	(1.4)	0.000032	(4.1)
$\sigma(\Omega_c h^2)$	0.0010	0.00078	(1.3)	0.00027	(3.7)
$\sigma(H_0)$	0.52	0.38	(1.4)	0.12	(4.3)
$\sigma(\tau)$	0.0042	0.0036	(1.1)	0.0023	(1.8)
$\sigma(n_S)$	0.0032	0.0024	(1.3)	0.0015	(2.1)
$\sigma(\log[10^{10} A_S])$	0.013	0.010	(1.3)	0.0055	(2.4)
$\sigma(p_{\rm ann})$	$<1.5 \cdot 10^{-7}$	$<1.3 \cdot 10^{-7}$	(1.2)	$<6.3 \cdot 10^{-8}$	(2.4)

TABLE VI. 68% C.L. errors on cosmological parameters in the case of helium abundance. The numbers in brackets show the improvement factor $\sigma_{\rm Planck}/\sigma$ with respect to the Planck experiment.

Parameter uncertainty	Planck	Planck + ACTPol		CMBPol	
$\sigma(\Omega_b h^2)$	0.00019	0.00015	(1.3)	0.000051	(3.7)
$\sigma(\Omega_c h^2)$	0.0010	0.00078	(1.3)	0.00027	(3.7)
$\sigma(\theta_S)$	0.00046	0.00032	(1.4)	0.00010	(4.6)
$\sigma(\tau)$	0.0043	0.0038	(1.1)	0.0023	(1.9)
$\sigma(n_S)$	0.0063	0.0051	(1.3)	0.0025	(2.5)
$\sigma(\log[10^{10}A_S])$	0.018	0.015	(1.2)	0.0079	(1.6)
$\sigma(Y_p)$	0.010	0.0072	(1.4)	0.0029	(3.4)

easy to see that the major impact of including this parameter is on the determination of the scalar spectral index n_s and the baryon abundance, with the 1-σ C.L. increased by a factor $\sim$2. In Figs. 8 and 9 we plot the two-dimensional likelihood contours at 68% and 95% C.L. between Y_p and these parameters.

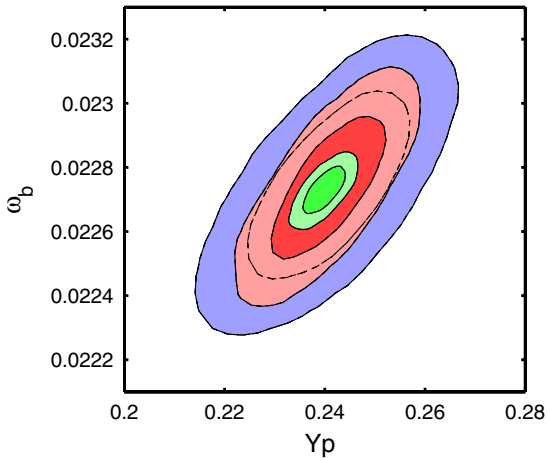

FIG. 8 (color online). 68% and 95% likelihood contour plots on the $Y_{\rm He}$–ω_b plane for Planck (blue), Planck + ACTPol (red), and CMBPol (green).

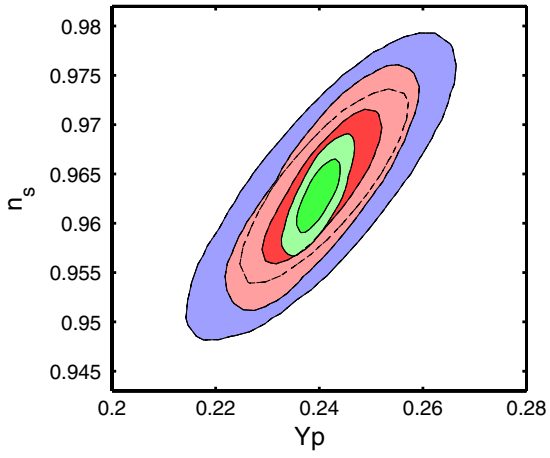

FIG. 9 (color online). 68% and 95% likelihood contour plots on the $Y_{\rm He}$–n_s plane for Planck (blue), Planck + ACTPol (red), and CMBPol (green).

F. Future constraints on dark energy equation of state

As is well known, primary CMB anisotropies are not able to provide accurate measurements of the dark energy equation of state because of geometrical degeneracies present with other parameters such as the amplitude of the dark energy density itself (see e.g. [57]) or the Hubble parameter. The tightest constraints on the dark energy equation of state are therefore provided by supernovae data combined with CMB data. The Union2 catalog of 557 supernovae [58] provides a constraint of $w = -0.999^{+0.074}_{-0.079}$ when systematic and statistical errors are considered. Nevertheless, combining CMB data with CMB lensing can also break degeneracies (see [59,60]) and provide interesting constraints, as already explored by several authors (see e.g. [61]) and as we can see in Table VII and from Fig. 10. It is interesting to notice that the error on w is strongly dominated by the degeneracy with H_0. In fact, the constraints on w from the three data sets considered are almost the same if one adds a strong prior on H_0 at a level of 2%, obtaining $\sigma(w) = 0.039$ for Planck, $\sigma(w) = 0.038$ for Planck + ACT, and $\sigma(w) = 0.033$ for CMBpol.

G. Future constraints on variations of fundamental constants

CMB anisotropies are sensitive to variations in fundamental constants such as the fine structure constant α (see e.g. [62–67]) or Newton's constant G ([68,69]) through changes in the recombination scenario.

Varying α changes the ionization and excitation rates and can delay or accelerate recombination. We have modified the RECFAST routine [48] in the CAMB code [26] in order to take into account this effect, following [64].

On the other hand, varying G does not affect recombination directly but "rescales" the expansion rate of the Universe, changing the epoch when recombination takes place. We have therefore redefined the gravitational constant in the CAMB code ([26]), as was also done in [68].

TABLE VII. 68% C.L. errors on cosmological parameters from future surveys in case of a variable dark energy equation of state w. The numbers in brackets show the improvement factor $\sigma_{\rm Planck}/\sigma$ with respect to the Planck experiment.

Parameter uncertainty	Planck	Planck + ACTPol		CMBPol	
$\sigma(\Omega_b h^2)$	0.00013	0.000093	(1.4)	0.000032	(4.2)
$\sigma(\Omega_c h^2)$	0.0011	0.00086	(1.3)	0.00038	(3.0)
$\sigma(\theta_s)$	0.00026	0.00019	(1.4)	0.000053	(4.9)
$\sigma(\tau)$	0.0040	0.0037	(1.1)	0.0023	(1.8)
$\sigma(n_s)$	0.0032	0.0025	(1.3)	0.0016	(2.0)
$\sigma(\log[10^{10}As])$	0.013	0.011	(1.2)	0.0070	(1.9)
$\sigma(w)$	0.20	0.17	(1.2)	0.085	(2.2)

TABLE VIII. 68% C.L. errors on cosmological parameters from future surveys in case of a variable gravitational constant G. The numbers in brackets show the improvement factor $\sigma_{\rm Planck}/\sigma$ with respect to the Planck experiment.

Parameter uncertainty	Planck	Planck + ACTPol		CMBPol	
$\sigma(\Omega_b h^2)$	0.00019	0.00015	(1.3)	0.000048	(3.9)
$\sigma(\Omega_c h^2)$	0.0010	0.00082	(1.2)	0.00025	(4.0)
$\sigma(\tau)$	0.0042	0.0039	(1.1)	0.0022	(1.9)
$\sigma(H_0)$	0.60	0.47	(1.3)	0.13	(4.6)
$\sigma(n_s)$	0.0061	0.0050	(1.2)	0.0023	(2.6)
$\sigma(\log[10^{10}A_s])$	0.018	0.015	(1.2)	0.0073	(2.5)
$\sigma(\lambda_G)$	0.012	0.0081	(1.5)	0.0030	(4.0)

The constraints are reported in Tables VIII and IX for variations in G and α, respectively. In order to parametrize the variations with dimensionless quantities, we have considered variations in the parameters $\Delta_\alpha = \alpha/\alpha_0$ and $\lambda_G = G/G_0$ where α_0 and G_0 are the current values of these fundamental constants, measured in the laboratory[3] $\alpha_0 = 7.297\,352\,537\,6(50) \times 10^{-3}$ and $G_0 = 6.674\,28(67) \times 10^{-11} m^3 kg^{-1} s^{-2}$.

As we can see from Tables VIII and IX, a variation in these fundamental constants has important effects for the determination of the scalar spectral index n_s and the Hubble constant H_0. This can also be seen in the two-dimensional likelihood contour plots in Figs. 11–14.

IV. DEGENERACIES

In the previous sections we presented the constraints on several parameters by considering the standard six Λ-CDM parameters plus one extra parameter at the time. However, if one lets more extra parameters to vary together, additional degeneracies between these parameters might weaken the constraints previously found. We therefore studied the combination of the extra parameters that might present the strongest degeneracies between them. Table X shows the constraints obtained for different combinations of parameters in the most relevant cases.

[3]See http://www.codata.org/.

Several authors have studied and forecasted the constraining power of CMB experiments on neutrino masses, alone or combined with different astrophysical probes and with or without lensing extraction for future CMB experiments [61,70–72]. WMAP7 has provided a quite stringent constraint on the sum of neutrino masses of $\sum m_\nu < 1.3$ eV at 95% C.L. [5]. This constraint is improved to $\sum m_\nu < 0.44$ eV at 95% C.L. when WMAP7 is combined with Sloan Digital Sky Survey data [73] and with the Hubble Space Telescope prior [74] on the Hubble constant.

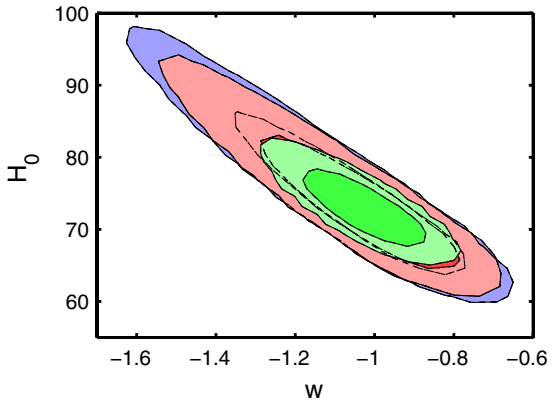

FIG. 10 (color online). 68% and 95% likelihood contour plots on the w–H_0 plane for Planck (blue), Planck + ACTPol (red), and CMBPol (green).

TABLE IX. 68% C.L. errors on cosmological parameters from future surveys in case of a variable fine structure constant α. The numbers in brackets show the improvement factor $\sigma_{\rm Planck}/\sigma$ with respect to the Planck experiment.

Parameter uncertainty	Planck	Planck + ACTPol		CMBPol	
$\sigma(\Omega_b h^2)$	0.00013	0.00011	(1.2)	0.000035	(4.1)
$\sigma(\Omega_c h^2)$	0.0012	0.00094	(1.3)	0.00032	(3.9)
$\sigma(\tau)$	0.0042	0.0037	(1.1)	0.0024	(1.8)
$\sigma(H_0)$	0.77	0.51	(1.5)	0.21	(3.8)
$\sigma(n_s)$	0.0060	0.0048	(1.3)	0.0026	(2.6)
$\sigma(\log[10^{10}A_s])$	0.015	0.015	(1.0)	0.0042	(2.5)
$\sigma(\alpha/\alpha_0)$	0.0018	0.0013	(1.4)	0.00053	(3.7)

Nevertheless, when also the number of effective relativistic particles $N_{\rm eff}$ and the dark energy equation of state w are sampled, these bounds relax of about a factor 2 (see [75] for a wider review on current bounds).

The well-known degeneracy between the sum of neutrino masses $\sum m_\nu$ and the number of relativistic species $N_{\rm eff}$ arises from the fact that a greater value of $N_{\rm eff}$ increases the amount of radiation density ω_r. In order to

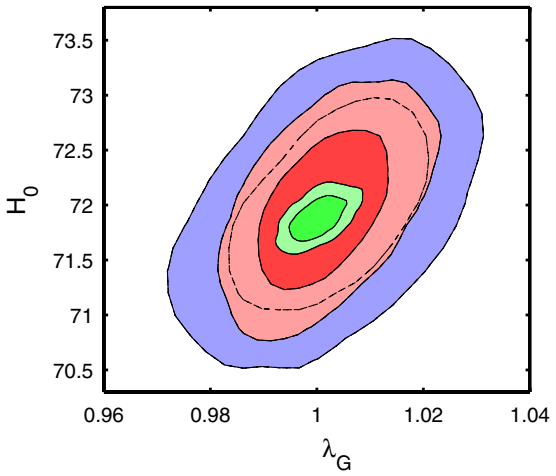

FIG. 11 (color online). 68% and 95% likelihood contour plots on the λ_G–H_0 plane for Planck (blue), Planck + ACTPol (red), and CMBPol (green).

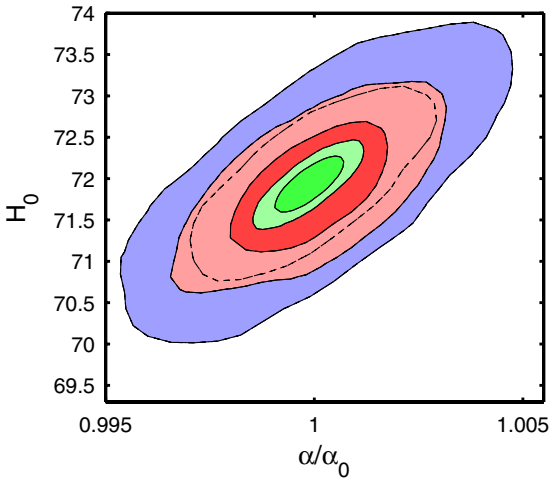

FIG. 13 (color online). 68% and 95% likelihood contour plots on the α/α_0–H_0 plane for Planck (blue), Planck + ACTPol (red), and CMBPol (green).

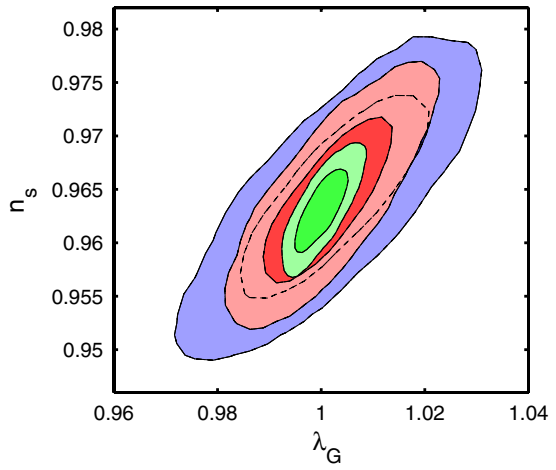

FIG. 12 (color online). 68% and 95% likelihood contour plots on the λ_G–n_s plane for Planck (blue), Planck + ACTPol (red), and CMBPol (green).

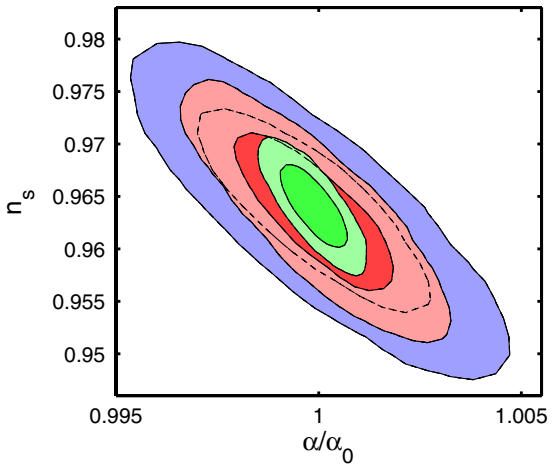

FIG. 14 (color online). 68% and 95% likelihood contour plots on the α/α_0–n_s plane for Planck (blue), Planck + ACTPol (red), and CMBPol (green).

TABLE X. 68% C.L. errors on cosmological parameters from future surveys when different combinations of parameters are let vary in addition to the six standard ΛCDM parameters. The entries for $\sum m_\nu$ are 68% C.L. upper limits, while the entries for $p_{\rm ann}$ are 95% upper limits. We performed the analysis for Planck only data in the case of ΛCDM + $\sum m_\nu$ + Yp and ΛCDM + $\sum m_\nu$ + $p_{\rm ann}$ as no significant degeneracies arose in these cases. The numbers in brackets show the improvement factor $\sigma_{\rm Planck}/\sigma$ with respect to the Planck experiment.

Parameter uncertainty	Planck	Planck + ACTPol		CMBPol	
		ΛCDM + $\sum m_\nu$ + $N_{\rm eff}$			
$\sigma(\sum m_\nu)$	<0.14	<0.10	(1.4)	<0.050	(2.8)
$\sigma(N_{\rm eff})$	0.11	0.091	(1.2)	0.033	(3.3)
		ΛCDM + Y_p + $N_{\rm eff}$			
$\sigma(Y_p)$	0.014	0.011	(1.3)	0.0048	(2.9)
$\sigma(N_{\rm eff})$	0.26	0.20	(1.3)	0.076	(3.4)
ΛCDM + $\sum m_\nu$ + Yp					
$\sigma(\sum m_\nu)$	<0.14	—		—	
$\sigma(Y_p)$	0.011	—		—	
ΛCDM + $\sum m_\nu$ + $p_{\rm ann}$					
$\sigma(\sum m_\nu)$	<0.16	—		—	
$\sigma(p_{\rm ann})$	1.7×10^{-7}	—		—	

maintain the redshift of equality between matter and radiation, $z_{eq} = \omega_m/\omega_r$, fixed to the value measured by CMB data, the amount of matter density ω_m also has to be increased. The consequence of that is an enhanced power of the matter power spectrum at small scales, that can be compensated by a larger neutrino mass that free-streams away the small scales perturbations. Using WMAP1 data, Crotty *et al.* [76] showed that priors and combination with large scale structure data are needed in order to break this degeneracy. Nevertheless, we checked that the improved quality of future data on small scales and the addition of lensing information partially breaks the degeneracy as well, as shown in Fig. 15. We fixed the number of massive neutrinos to 3 and let vary the additional possible number of relativistic species, together with the mass of neutrinos. The overall uncertainties on all the parameters are, however, still increased when both the parameters are let vary, as shown in Table XI.

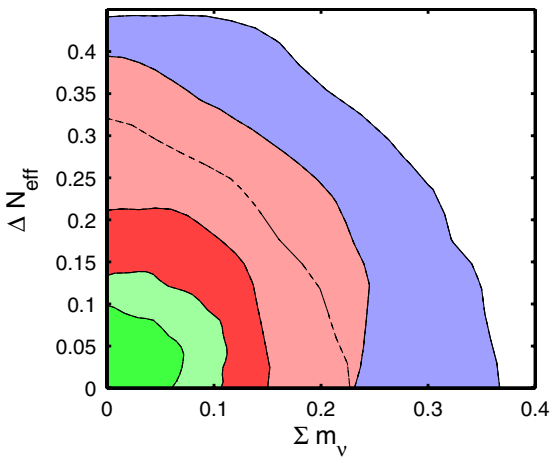

FIG. 15 (color online). 68% and 95% likelihood contour plots on the $\Delta N_{\rm eff}$–$\sum m_\nu$ plane for Planck (blue), Planck + ACTPol (red), and CMBPol (green). We define $\Delta N_{\rm eff} = N_{\rm eff} - 3$, as we fixed the number of massive neutrinos to 3.

Several authors also studied the large degeneracy existing between $\sum m_\nu$ and the dark energy equation of state w [71,72,77]. This degeneracy arises from the fact that both $\sum m_\nu$ and w are degenerate with the matter density Ω_m. CMB alone cannot place significant constraints in this case and it must be combined with external data such as supernovae and baryon acoustic oscillations data [4] in order to provide meaningful limits. This analysis is therefore beyond the scope of this paper.

We also checked that no strong degeneracies seem to arise when $\sum m_\nu$ and the fraction of helium abundance Y_p are considered together, as shown in Fig. 16, as well as when $\sum m_\nu$ is varied together with the parameter of annihilation $p_{\rm ann}$.

On the contrary, a degeneracy is known to arise between the number of relativistic species $N_{\rm eff}$ and the abundance of primordial Y_p [54,55,78], as shown in Fig. 17. This degeneracy weakens the constraints on the two parameters of about ~40%, as shown in Table X.

As the variation of fundamental constants is concerned, the effect of a variable fine structure constant is partially degenerate with the one caused by the gravitational constant on CMB spectra, as shown in [65]. Nevertheless, Planck will partially break this degeneracy thanks to its improved EE polarization data. It must be noted, however, that this degeneracy might hide a real correlation between the value of the two couplings, due to some underlying common mechanism, such as the presence of a new unknown scalar field, responsible for the variation of the two quantities. This encourages very interesting possibilities and further studies in the future.

TABLE XI. 68% C.L. errors on cosmological parameters from future surveys in case of a variable sum of neutrino masses $\sum m_\nu$ and number of relativistic species $N_{\rm eff}$. The numbers in brackets show the improvement factor $\sigma_{\rm Planck}/\sigma$ with respect to the Planck experiment. The entries for $\sum m_\nu$ are upper limits at 68% C.L.

Parameter uncertainty	Planck	Planck + ACTPol		CMBPol	
$\sigma(\Omega_b h^2)$	0.00016	0.00013	(1.2)	0.000041	(3.9)
$\sigma(\Omega_c h^2)$	0.0022	0.0017	(1.3)	0.00076	(2.9)
$\sigma(\theta_s)$	0.00035	0.00025	(1.4)	0.000074	(4.7)
$\sigma(\tau)$	0.0043	0.0037	(1.2)	0.0023	(1.9)
$\sigma(n_s)$	0.0051	0.0043	(1.2)	0.0023	(2.2)
$\sigma(log[10^{10}A_s])$	0.016	0.013	(1.2)	0.0078	(2.0)
$\sigma(\sum m_\nu)$	<0.14	<0.10	(1.4)	<0.050	(2.8)
$\sigma(N_{\rm eff})$	0.11	0.091	(1.2)	0.033	(3.3)

V. CONCLUSIONS

In this paper we have performed a systematic analysis of the future constraints on several parameters achievable from CMB experiments. Aside from the six parameters of the standard Λ-CDM model we have considered new parameters mostly related to quantities which can be probed in a complementary way in the laboratory and/or with astrophysical measurements. In particular we found that the Planck experiment will provide bounds on the sum of the masses Σm_ν that could potentially definitively confirm or rule out the Heidelberg-Moscow claim for a detection of an absolute neutrino mass scale. Planck + ACTPol could reach sufficient sensitivity for a robust detection of neutrino mass for an inverted hierarchy, while CMBPol should also be able to detect it for a direct mass hierarchy. The comparison of Planck + ACTPol constraints on baryon density $N_{\rm eff}$ and Y_p with the complementary bounds from big bang nucleosynthesis will provide a fundamental test for the whole cosmological scenario. CMBPol could have a very important impact in understanding the epoch of neutrino decoupling. Moreover, the primordial helium abundance can be constrained with an accuracy equal to that of current astrophysical measurements but with much better control of systematics. Constraints on fundamental constants can be achieved at a level close to laboratory constraints. Such overlap between cosmology and other fields of physics and astronomy is one of the most interesting aspects of future CMB research.

We should note, however, that our forecasts rely on several technical assumptions. First, we assumed that the theoretical model of the recombination process is accurately known. This is not quite true as corrections to the recombination process are already needed for the Planck experiment (see e.g. [79]). However, this is mainly a computational problem that could be solved by the time of CMBPol launch, expected not before 2015. In addition, we assume that the foreground and beam uncertainties are smaller than the statistical errors.

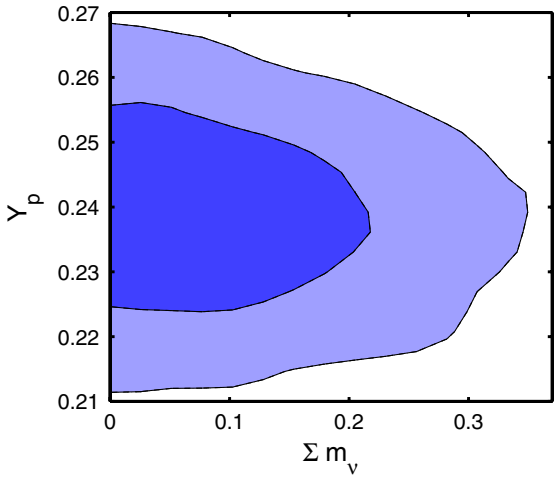

FIG. 16 (color online). 68% and 95% likelihood contour plots on the $\sum m_\nu$–Y_p plane for Planck data.

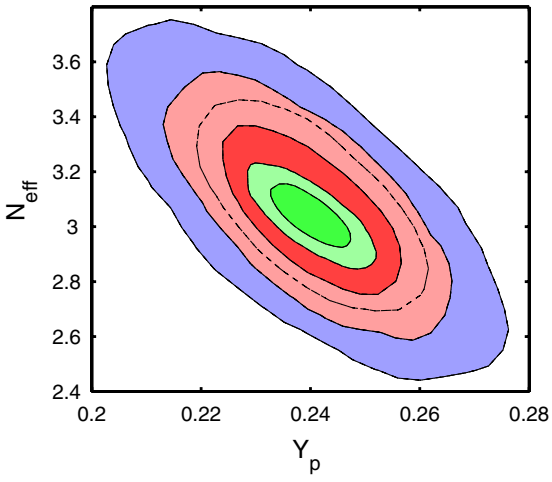

FIG. 17 (color online). 68% and 95% likelihood contour plots on the Y_p–$N_{\rm eff}$ plane for Planck data (blue), Planck + ACTPol (red), and CMBPol (green).

Finally, degeneracies arising when more than one extra parameter is let vary at the same time can weaken the constraints found when only one extra parameter is considered. In this case, the combination of CMB data with additional complementary probes is essential to break the degeneracies.

Nevertheless, the results clearly show the advantage of adding small-scale data from the ACT telescope to the Planck satellite data. Adding the former to the latter, the parameter constraints should improve by about 20%–40%.

ACKNOWLEDGMENTS

This research has been supported by ASI Contract No. I/016/07/0 "COFIS." B. S. is supported by NSF. D. N. S. is supported by NASA theory Grant No. NNX087AH30G and NSF Grant No. 0707731.

[1] G. F. Smoot *et al.*, Astrophys. J. **396**, L1 (1992); C. L. Bennett *et al.*, Astrophys. J. **464**, L1 (1996).
[2] A. D. Miller *et al.*, Astrophys. J. **524**, L1 (1999); A. Melchiorri *et al.* (Boomerang Collaboration), Astrophys. J. **536**, L63 (2000); P. de Bernardis *et al.* (Boomerang Collaboration), Nature (London) **404**, 955 (2000); S. Hanany *et al.*, Astrophys. J. **545**, L5 (2000); N. W. Halverson *et al.*, Astrophys. J. **568**, 38 (2002); C. L. Reichardt *et al.*, Astrophys. J. **694**, 1200 (2009); Astrophys. J. **716**, 1040 (2010); J. L. Sievers *et al.*, arXiv:0901.4540; M. L. Brown *et al.*, Astrophys. J. **705**, 978 (2009); N. R. Hall *et al.*, Astrophys. J. **718**, 632 (2010); S. Das *et al.*, arXiv:1009.0847.
[3] D. N. Spergel *et al.* (WMAP Collaboration), Astrophys. J. Suppl. Ser. **148**, 175 (2003); C. L. Bennett *et al.* (WMAP Collaboration), Astrophys. J. Suppl. Ser. **148**, 1 (2003);
[4] E. Komatsu *et al.*, Astrophys. J. Suppl. Ser. **180**, 330 (2009).
[5] E. Komatsu, arXiv:1001.4538.
[6] J. Tauber *et al.* (Planck Collaboration), arXiv:astro-ph/0604069.
[7] M. J. White, Astrophys. J. **555**, 88 (2001); A. Cooray, arXiv:astro-ph/0203048.
[8] U. Seljak and M. Zaldarriaga, Phys. Rev. Lett. **78**, 2054 (1997); M. Kamionkowski, A. Kosowsky, and A. Stebbins, Phys. Rev. D **55**, 7368 (1997).
[9] P. Oxley *et al.*, Proc. SPIE Int. Soc. Opt. Eng. **5543**, 320 (2004).
[10] M. D. Niemack *et al.*, Proc. SPIE Int. Soc. Opt. Eng. **Vol.**, 77411S (2010).
[11] A. Kosowsky (ACT Collaboration), New Astron. Rev. **50**, 969 (2006).
[12] J. E. Carlstrom *et al.*, arXiv:0907.4445.
[13] J. Bock *et al.* (CMBPol Collaboration), arXiv:0906.1188.
[14] P. de Bernardis, M. Bucher, C. Burigana, and L. Piccirillo (f. P. Collaboration), Exp. Astron. **23**, 5 (2008).
[15] M. Zaldarriaga and U. Seljak, Phys. Rev. D **58**, 023003 (1998); A. Lewis and A. Challinor, Phys. Rep. **429**, 1 (2006).
[16] C. M. Hirata and U. Seljak, Phys. Rev. D **68**, 083002 (2003);
[17] T. Okamoto and W. Hu, Phys. Rev. D **67**, 083002 (2003).
[18] L. P. L. Colombo, E. Pierpaoli, and J. R. Pritchard, Mon. Not. R. Astron. Soc. **398**, 1621 (2009).
[19] H. Li *et al.*, Phys. Lett. B **675**, 164 (2009).
[20] M. Shimon, N. J. Miller, C. T. Kishimoto, C. J. Smith, G. M. Fuller, and B. G. Keating, J. Cosmol. Astropart. Phys. 05 (2010) 037.
[21] D. Baumann *et al.* (CMBPol Study Team Collaboration), AIP Conf. Proc. **1141**, 10 (2009).
[22] M. Zaldarriaga *et al.*, arXiv:0811.3918.
[23] S. Dodelson *et al.*, arXiv:0902.3796.
[24] L. Perotto, J. Lesgourgues, S. Hannestad, H. Tu, and Y. Y. Y. Wong, J. Cosmol. Astropart. Phys. 10 (2006) 013.
[25] J. Dunkley *et al.* (WMAP Collaboration), Astrophys. J. Suppl. Ser. **180**, 306 (2009).
[26] A. Lewis, A. Challinor, and A. Lasenby, Astrophys. J. **538**, 473 (2000).
[27] A. Lewis and S. Bridle, Phys. Rev. D **66**, 103511 (2002).
[28] J. W. Fowler *et al.* (The ACT Collaboration), Astrophys. J. **722**, 1148 (2010).
[29] M. Lueker *et al.*, Astrophys. J. **719**, 1045 (2010).
[30] J. Dunkley *et al.*, AIP Conf. Proc. **1141**, 222 (2009).
[31] C. P. Ma and E. Bertschinger, Astrophys. J. **455**, 7 (1995).
[32] K. Ichikawa, M. Fukugita, and M. Kawasaki, Phys. Rev. D **71**, 043001 (2005).
[33] K. Abazajian and S. Dodelson, Phys. Rev. Lett. **91**, 041301 (2003).
[34] A. Slosar, Phys. Rev. D **73**, 123501 (2006).
[35] M. Kaplinghat, L. Knox, and Y. S. Song, Phys. Rev. Lett. **91**, 241301 (2003).
[36] G. L. Fogli *et al.*, Phys. Rev. D **78**, 033010 (2008).
[37] M. Beck (Katrin Collaboration), J. Phys. Conf. Ser. **203**, 012097 (2010).
[38] J. R. Kristiansen and O. Elgaroy, J. Cosmol. Astropart. Phys. 01 (2008) 007.
[39] H. V. Klapdor-Kleingrothaus, I. V. Krivosheina, A. Dietz, and O. Chkvorets, Phys. Lett. B **586**, 198 (2004).
[40] A. Monfardini *et al.*, Nucl. Instrum. Methods Phys. Res., Sect. A **559**, 346 (2006).
[41] R. Bowen, S. H. Hansen, A. Melchiorri, J. Silk, and R. Trotta, Mon. Not. R. Astron. Soc. **334**, 760 (2002).
[42] G. Mangano, G. Miele, S. Pastor, and M. Peloso, Phys. Lett. B **534**, 8 (2002).
[43] G. Mangano, G. Miele, S. Pastor, T. Pinto, O. Pisanti, and P. D. Serpico, Nucl. Phys. **756B**, 100 (2006).
[44] S. Galli, F. Iocco, G. Bertone, and A. Melchiorri, Phys. Rev D. **80**, 023505 (2009).

[45] L. Zhang, X. L. Chen, Y. A. Lei, and Z. G. Si, Phys. Rev. D **74**, 103519 (2006); L. Zhang, X. Chen, M. Kamionkowski, Z. g. Si, and Z. Zheng, Phys. Rev. D **76**, 061301 (2007).
[46] X. Chen and M. Kamionkowski, Phys. Rev D. **70**, 043502 (2004).
[47] N. Padmanabhan and D. P. Finkbeiner, Phys. Rev D. **72**, 023508 (2005).
[48] S. Seager, D. D. Sasselov, and D. Scott, Astrophys. J. **523**, L1 (1999), http://www.astro.ubc.ca/people/scott/recfast.html.
[49] O. Adriani *et al.*, Nature (London) **458**, 607 (2009).
[50] J. Chang *et al.*, Nature (London) **456**, 362 (2008).
[51] L. Latronico (Fermi LAT Collaboration), arXiv:0907.0452.
[52] T. R. Slatyer, N. Padmanabhan, and D. P. Finkbeiner, Phys. Rev D **80**, 043526 (2009).
[53] R. Trotta and S. H. Hansen, Phys. Rev. D **69**, 023509 (2004).
[54] K. Ichikawa, T. Sekiguchi, and T. Takahashi, Phys. Rev. D **78**, 043509 (2008).
[55] J. Hamann, J. Lesgourgues, and G. Mangano, J. Cosmol. Astropart. Phys. 3 (2008) 4.
[56] F. Iocco, G. Mangano, G. Miele, O. Pisanti, and P. D. Serpico, Phys. Rep. **472**, 1 (2009).
[57] R. Bean and A. Melchiorri, Phys. Rev. D **65**, 041302 (2002).
[58] R. Amanullah, Astrophys. J. **716**, 712 (2010).
[59] W. Hu, Phys. Rev. D **65**, 023003 (2001).
[60] G. Efstathiou and J. R. Bond, Mon. Not. R. Astron. Soc. **304**, 75 (1999).
[61] K. M. Smith, W. Hu, and M. Kaplinghat, Phys. Rev. D **74**, 123002 (2006); L. Hollenstein, D. Sapone, R. Crittenden, and B. M. Schaefer, J. Cosmol. Astropart. Phys. 04 (2009) 012; W. Hu, D. Huterer, and K. M. Smith, Astrophys. J. **650**, L13 (2006).
[62] S. Hannestad, Phys. Rev D **60**, 023515 (1999).
[63] M. Kaplinghat, R. J. Scherrer, and M. S. Turner, Phys. Rev D **60**, 023516 (1999).
[64] E. Menegoni, S. Galli, J. G. Bartlett, C. J. A. P. Martins, and A. Melchiorri, Phys. Rev D **80**, 087302 (2009)
[65] C. J. A. P. Martins, E. Menegoni, S. Galli, G. Mangano, and A. Melchiorri, Phys. Rev. D **82**, 023532 (2010).
[66] K. Ichikawa, T. Kanzaki, and M. Kawasaki, Phys. Rev D **74**, 023515 (2006).
[67] S. J. Landau and C. G. Scóccola, arXiv:1002.1603.
[68] S. Galli, A. Melchiorri, G. F. Smoot, and O. Zahn, Phys. Rev D **80**, 023508 (2009); O. Zahn and M. Zaldarriaga, Phys. Rev. D **67**, 063002 (2003).
[69] K. i. Umezu, K. Ichiki, and M. Yahiro, Phys. Rev. D **72**, 044010 (2005).
[70] J. Q. Xia, G. B. Zhao, and X. Zhang, Phys. Rev. D **75**, 103505 (2007); L. P. L. Colombo, E. Pierpaoli, and J. R. Pritchard, Mon. Not. R. Astron. Soc. **398**, 1621 (2009).
[71] R. de Putter, O. Zahn, and E. V. Linder, Phys. Rev. D **79**, 065033 (2009).
[72] S. Hannestad, Phys. Rev. Lett. **95**, 221301 (2005).
[73] B. A. Reid *et al.*, Mon. Not. R. Astron. Soc. **404**, L60 (2010).
[74] A. G. Riess *et al.*, Astrophys. J. **699**, 539 (2009).
[75] S. Hannestad, Prog. Part. Nucl. Phys. **65**, 185 (2010).
[76] P. Crotty, J. Lesgourgues, and S. Pastor, Phys. Rev D **69**, 123007 (2004).
[77] A. De La Macorra *et al.*, Astropart. Phys. **27**, 406 (2007).
[78] J. Dunkley *et al.*, arXiv:1009.0866.
[79] J. A. Rubino-Martin, J. Chluba, W. A. Fendt, and B. D. Wandelt, arXiv:0910.4383.
[80] I. Cholis, G. Dobler, D. P. Finkbeiner, L. Goodenough, and N. Weiner, Phys. Rev D **80**, 123518 (2009).
[81] P. Grajek, G. L. Kane, D. J. Phalen, A. Pierce, and S. Watson, Phys. Rev D **79**, 043506 (2009).